

RELATIONSHIP BETWEEN FRACTURE TOUGHNESS AND RELATIVE DENSITY IN IRON AND COPPER METAL POWDER COMPACTS

A. A. Alabi^{*1}, S. M. Tahir², M. A. Azmah Hanim², N. I. Zahari² and M. S. Anuar³

¹ Department of Mechanical Engineering, Faculty of Engineering, Ahmadu Bello University, P.M.B. 1045 Samaru- Zaria, Kaduna, Nigeria

² Department of Mechanical and Manufacturing Engineering, Faculty of Engineering, Universiti Putra Malaysia, 43400 UPM Serdang, Selangor, Malaysia

³ Department of Process and Food Engineering, Faculty of Engineering, Universiti Putra Malaysia, 43400 UPM Serdang, Selangor, Malaysia

* Corresponding Author's Email: aalabi@abu.edu.ng; abdulmm2001@gmail.com

ABSTRACT

Iron and copper powders are the two most commonly used metallic raw materials for components formation in the powder metallurgy (PM) industry. The quality of a PM component depends on the ability to achieve high green strength. Most PM components are susceptible to fracture failure due to unpredictable crack propagation and inhomogeneous density distribution. In this paper, we examined the influence of the relative density of green iron and copper powder compacts on the rate of crack propagation due to shear loading, or the mode II fracture toughness (K_{IIC}). The integrated uniaxial compaction of a fixed amount of loose powder method was used to produce the modified diametrical compression test technique (MDCTT) samples used to evaluate the K_{IIC} of the two metal powder compacts studied. The rate of the in-plane crack propagation in the powder compacts slows down as the powder compacts became denser. The inverse of the fracture toughness, $\frac{1}{K_{IIC}}$ was found to be related to $\frac{1}{1 - \ln(\rho_r)}$ by constants that are unique to each of the powders. The constants are 33.2 for the iron powder compacts and 55.5 for the copper powder compacts. Furthermore, the constants were found to be related to the coefficients of thermal expansivity for solid iron and solid copper. This study has provided a mathematical relation that can be used to estimate the K_{IIC} for iron and copper based powder compacts from their relative densities. The mathematical relation is also capable of providing useful information about the thermal properties of the related metals.

Keywords: Fracture toughness, relative density, metal powder compact, compression test.

INTRODUCTION

The quality of a powder metallurgy (PM) component depends on the quality of its green compact. For metal powder compacts, the two most critical properties to achieving green compacts of high quality are density or relative density and strength. The influence of green density on critical properties of PM components such as strength and hardness has been extensively studied. Researchers have established that improved green density leads to increase in the green strength of metal powder compacts King, *et al.* (2005); Tahir *et al.* (2010); Degnan *et al.* (2004); Jonsén *et al.* (2007). In uniaxial compaction of powders, density of components is largely determined by compaction pressure Khuntia and Pani (2018); Poquillon *et al.* (2002); Heckel (1961); Hwang and Kobayashi (1990); Enneti *et al.* (2013); Solimanjad and Larsson (2003); King *et al.* (2005). Zhou *et al.* (2017) reported that there was variation in the relative density of Ag 57.6-Cu22.4-Sn10-In10 powder compacted uniaxially in a rigid column-like die. The authors of the paper showed that the relative density has a direct influence on the radial tensile and the axial compressive strength of the powder. Akseli *et al.* (2011) used a non-destructive technique known as ultrasonic and X-ray tomography method to show that the density distribution in microcrystalline cellulose powder compacted using roller was inhomogeneous. They also show that the tensile strength of the powder compacts increase as the density increased.

Yohannes *et al.* (2015) studied the effect of fine particles on the strength of two pharmaceutical tableting powders that were compacted uniaxially. The powders are microcrystalline cellulose and lactose monohydrate. They also reported that the tensile strength of these powders increased with relative densities. Degnan *et al.* (2004) studied the green strength of compacts of two iron powders, Astaloy CrM and Distaloy AE Densmix. The powders were uniaxially compacted at room temperature and 130°C. The results showed that the green strength of both powder compacts appreciated as their relative densities increased. Tahir *et al.* (2010) also reported that the green strength of iron powder compacts increased with increase in relative density. Hare *et al.* (2018) studied some mechanical properties of compacts of a pharmaceutical powder known as Avicel PH102 that were broken under impact load. An equal mass of the powder was compacted in a 10 mm diameter die. It was reported that the Vickers hardness values varied on the top surface across the diameter of the tablet. This variation was attributed to the inhomogeneous nature of the density of the tablet. May *et al.* (2013) used a digital imaging technique known as Terahertz Pulsed Imaging to study the hardness and density distributions of two pharmaceutical tablets produced by powder compaction. The density was reported to increase laterally away from the centre of the tablets. The hardness of the tablets was found to increase with the increase in density.

Khuntia and Pani (2018) compacted equal mass of low carbon ferrous powders uniaxially at pressures ranging from 200 to 600 MPa and showed that the hardness values of the compacts rise with increasing density. Shi *et al.* (2017) investigated the mechanical properties of green and sintered compacts of 17-4PH stainless steel powders. Their findings showed that pre-sintering heating lowers the relative densities and hardness values of the compacts. However, the hardness values increased with the rise in relative density. Similarly, He *et al.* (2018) reported inhomogeneity in zirconia powder compacts used for dental prostheses. The zirconia powder compact was produced via injection molding, and the density was said to vary in the direction of ejection of the compact. The Vickers hardness value was also shown to vary on the surface of the compact as the density varied.

Powder compacts are products of a well-established sequence of events which include powder transfer and die filling, compaction, ejection, and post-ejection handling. According to Garner *et al.* (2014), cracks can form in a powder compact at any stage in this sequence but Tahir *et al.* (2010) reported that the likelihood is higher during compaction, when inter-particle bond formed is weak or not formed, and during ejection when the formed bonds are broken. Cracks in metal compacted components are the primary cause of fracture failure during service. One parameter used by design engineers and material scientist to predict the ability of a component to resist fracture failure in the presence of cracks is fracture toughness. Studies on the influence of density on the fracture toughness of green metal powder compacts are scanty in literature. Moshtaghion *et al.* (2016) examined the influence of grain size on the hardness and fracture toughness of almost 100% dense boron carbide ceramics. Four different ceramic powder samples were compacted and sintered at temperatures between 1600 and 1800°C. The fracture toughness was measured using the four-point bending test arrangement while density was measured by Archimedes principle. Their result showed that, for two of the boron carbide samples that were subjected to the same sintering temperature of 1700°C, the fracture toughness reduced from 2.6 to 2.5 MPa.m^{0.5} as their relative density increased from 98.5 to 100%. In another study on the densification and mechanical properties of boron carbide ceramics sintered at temperatures ranging from 1100 to 1800°C and soaked at different holding times where fracture toughness was determined using Vickers indenter, Sairam *et al.* (2014) reported that fracture toughness could not be measured for samples sintered between 1100 and 1600°C even though density increased from 60 to 81.8%. However, between the sintering temperature of 1700 and 1800°C, increase in relative density led to a reduction in fracture toughness. The results of Sairam *et al.* (2014) corroborated the finding reported by Moshtaghion *et al.* (2013) working with fine-grained boron carbide powders and using a similar method. Moshtaghion *et al.* (2013) showed that for sintering temperature between 1600 and 1700°C, relative density rose from 90.3 to 100% while fracture toughness fell from 4.81 to 3.65 MPa.m^{0.5}. Xiaorong *et al.* (2017) also upheld the assertion by the earlier mentioned authors that the fracture toughness of sintered boron carbide ceramics decreases with increase in

relative density. Contrary to the inverse relationship between relative density and fracture toughness of boron carbide ceramics reported by the researchers above, Chen *et al.* (2018) showed that the addition of graphene platelets to boron carbide powder produced sintered ceramics in which increase density resulted in improved Vickers indenter fractured toughness. This direct relation was true for sintering temperatures between 1725 to 1800°C. Farahbakhsh *et al.* (2017) studied the influence of density on the fracture toughness on a different type of ceramic powder; ZrB₂-SiC powder. This powder was doped with nano-sized carbon and hot pressed. The ceramic was sintered at 1850°C, fracture toughness was measured using the Vickers indentation method, and density was measured from the Archimedes principle. Their results showed a steady increase in fracture toughness as the relative density increased from 90.1 to 99.8%. Guha Roy *et al.* (2017) collected data on the mode I fracture toughness, tensile strength, uniaxial compressive strength and densities of rocks from twenty-six works published between 1983 and 2016. The data represented nine types of rocks. Only four of the rocks had both density and fracture toughness mentioned. The rocks had no common parameter since they were studied under different conditions. The tensile strength varied between 5.4 and 24.5 MPa, the uniaxial compressive strength ranged from 33 to 145.2 MPa, the mode I fracture toughness ranged from 0.3 and 3.19 MPa.m^{0.5} while the density of the only four rocks listed was between 2200 and 2579 kg/m³. However, the author concluded that the fracture toughness of rocks increases as density increases and that the two parameters are related power law equation. It is erroneous to put forward a generalized equation for when the parameters are not measured under the same conditions. Fleck and Smith (1981) studied the effect of density of the fracture toughness of sintered steel and found that the fracture toughness of the steel sample increases as the density increase. They reported that the values of the fracture toughness rose from 22 to 26 MPa.m^{0.5} as the density climbed from 6580 to 6980 kg.m⁻³. The fracture toughness test was conducted using the three-point bending test and in accordance with the 1978 version of ASTM E1820-01 (2001). It is evident from the largeness of the values of the fracture toughness that the steel sample studied by Fleck and Smith (1981) was not a green product powder metallurgy. The first study that reported the influence of relative density on the fracture toughness of a metal powder compact was by Tahir and Ariffin (2006). The study developed displacement-based finite element model that simulated the fracture initiation and propagation in a rotational flange component produced from iron powder and showed that fracture toughness increased as the values of the relative density appreciated. It is not surprising that only a few researchers have worked the fracture toughness of metal powder components. It is not surprising that only a few studies have mentioned on the fracture toughness of metal powder components. The popularity of the indentation fracture toughness test such as the Vickers indenter to measure the fracture toughness of ceramics is due to convenience Quinn and Bradt (2007). Rocha-Rangel (2011) reported that validity of the indentation fracture toughness test is limited to materials whose fracture toughness is greater than 1.0 MPa.m^{0.5} and whose structures are highly

homogeneous. Metal powder compacts produced by uniaxial compaction technique are known to have inhomogeneous structures. The mode I fracture toughness of iron powder compact was reported to be less than $1.0 \text{ MPa}\cdot\text{m}^{0.5}$ Degnan *et al.* (2004). The sample configuration for the three-point bending test and the four point bending test for measure fracture toughness as described in ASTM E1820-01 (2001) can only be achieved by materials with sufficiently high strength to withstand the rigor of different machining operations. Most green metal powder compacts have relative low strength. A method that has been successfully used to measure the fracture toughness of rock materials, concretes and other low strength materials is the diametrical compression test technique (DCTT). Literature shows that Degnan *et al.* (2004) was the first to measure the mode I fracture toughness, K_{IC} , of green iron powder compacts using the DCTT. The DCTT sample used by Degnan *et al.* was proposed by Szendi-Horvath in 1980, (Figure 1). Szendi-Horvath (1980) used the DCTT to measure the K_{IC} of two low strength materials, soda glass and Perspex while Clobes and Green (2002) used the same technique and Equation (1) to determine the K_{IC} of porous alumina. Alabi *et al.* (2017) modified the DCTT and developed a test method known as the modified diametrical compression test technique (MDCTT), see Figure 2. The MDCTT measures the mode II fracture toughness, K_{IIC} , of green iron and copper powder compacts from Equation (2) Alabi *et al.* (2017). With the success of the DCTT and the MDCTT in measuring the fracture toughness of green metal powder compacts there is the need to examine the relationship between relative density and the fracture toughness of the compacts. According to Alabi *et al.* (2017), the relationship between t_1 and t_2 for iron powder compacts (IPCs) and copper powder compacts (CPCs) is depicted by Equation (3) and Equation (4) respectively.

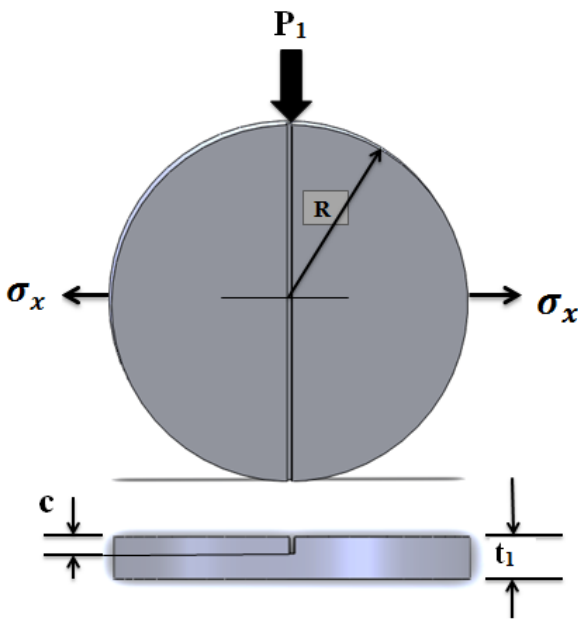


Figure 1: The DCTT setup

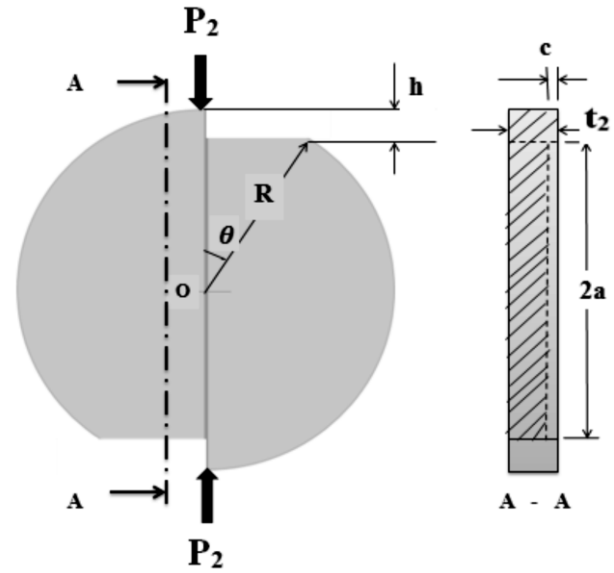


Figure 2: The MDCTT setup

$$K_{IC} = \frac{2.24}{D t_1} \frac{P_1 \sqrt{c}}{\sqrt{\pi}} \quad (1)$$

where, D is the diameter of compact, t_1 is the thickness of compact, P_1 is the maximum load at failure, and c = depth of the notch.

$$K_{IIC} = \frac{2\beta P_2}{(1-2\mu)\mu t_2 \sqrt{\pi}} \left\{ \frac{1}{[\sqrt{1+\beta^2}]^4} + \frac{(2\gamma-1)^2}{[\sqrt{(2\gamma-1)^2+\beta^2}]^4} \right\} \frac{(t_1-c)\sqrt{c}}{D(t_2-c)} \quad (2)$$

where, P_2 is the maximum load at the fracture of the MDCTT sample, c is the depth of the notch, $D=2R$ is the diameter of the compact and h is the rise above the flat cut on the MDCTT sample (Figure 2). $\beta = w/h$, $\mu = h/D$, $\gamma = R/h$. Where w is half the width of the notch.

$$t_1 = 1.181t_2 - 1.868 \quad (3)$$

$$t_1 = 0.765t_2 - 0.0374 \quad (4)$$

In this paper, we examined the relationship between the relative density and the mode II fracture toughness of two metal powder compacts, iron and copper.

METHODOLOGY

The materials used in this study are Hoaganas ASC 100.29 iron powder and pure copper powder. The powder were supplied by Sumitomo electric sintered components Malaysia. Table 1 shows some of the properties of the powders while Figure 3 depicts the morphology of the powders.

Table 1: Properties of the Iron and Copper powders

Parameter	Iron powder (Hoganas ASC 100.29)	Copper powder
Chemical Properties	C = 0.002%, O = 0.13%, Fe is base	Sn ≤ 0.1%, Pb = 0.003%, Loss in H = 0.16 %, Cu = 99.7%
Green Density (GD) @ 600 MPa, g/cm ³	7.13	-
Particle Size Distribution	<45µm = 23.7%, <75 µm = 27.4%, <150 µm = 41.7%, <180 µm = 6.6%, >180 µm = 0.6%, >212 µm = 0%	<45µm = 73.58%, >45µm = 26.10%, >75 µm = 0.20%, >106 µm = 0.03%

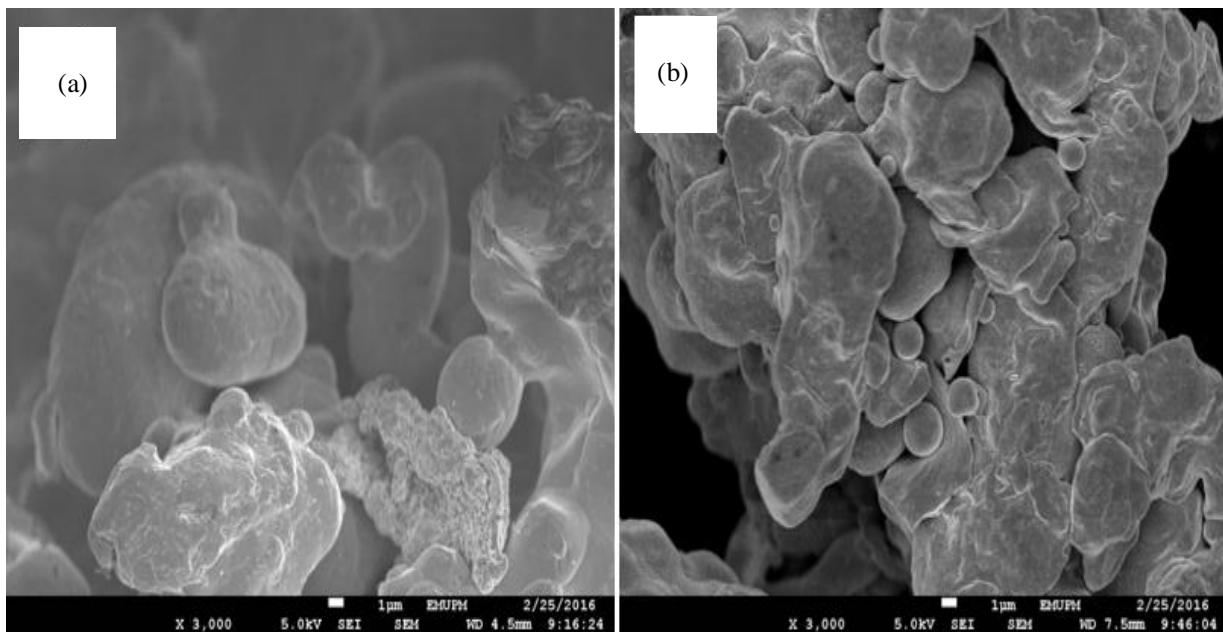


Figure 3: Morphology of the (a) Iron powder (b) Copper powder

A measured amount of each of metal powders was compressed in a rigid steel die specially designed to produce the modified diametrical compression test technique test (MDCTT) samples. The MDCTT samples were used to determine the mode II fracture toughness of the powder compacts. The basic components of the die and the dimensions of the mold are shown in Figure 4.

The production of the MDCTT sample adopts an integrated uniaxial compression and notching technique. This method eliminates the need for machining of the test samples since the required notch on each sample is produced during the compaction process. A fixed mass of metal powder is compressed uniaxially in the die (see Figure 5) to produce the MDCTT sample shown in Figure 1. The die is equipped with a ‘rail’ and ‘ways’ that gives the MDCTT sample its unique feature.

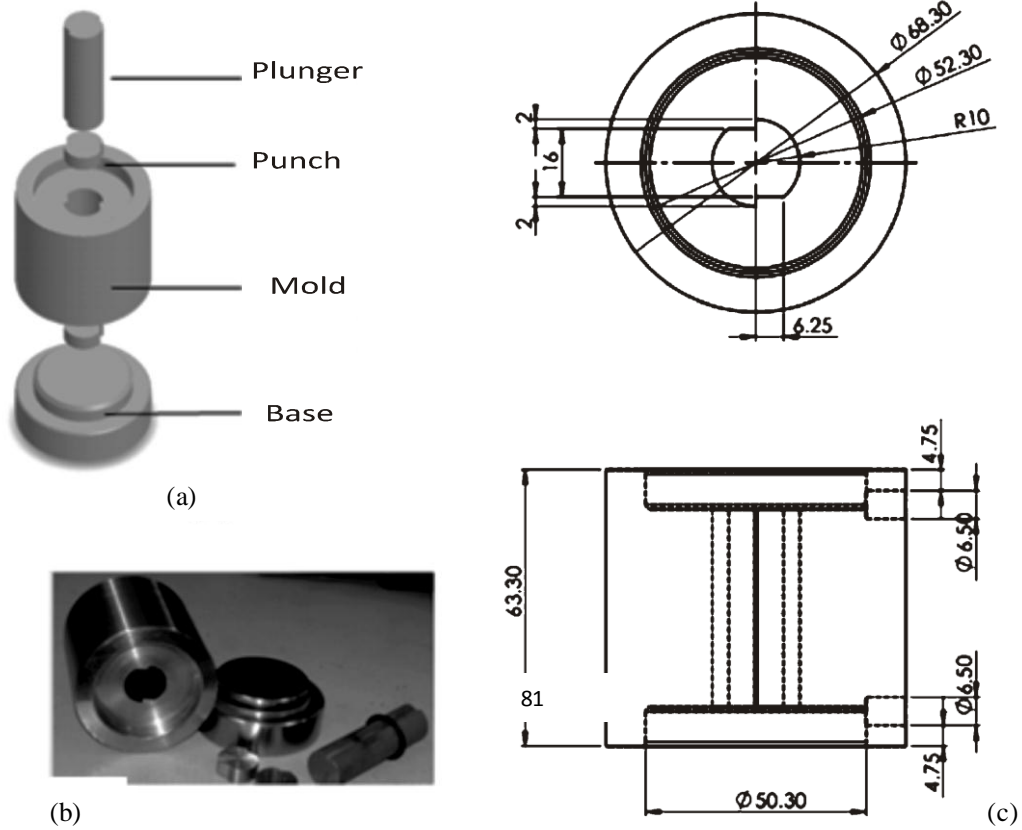


Figure 4: (a) View with parts named (b) pictorial view of the MDCTT die and (c) 2-D view of the mold

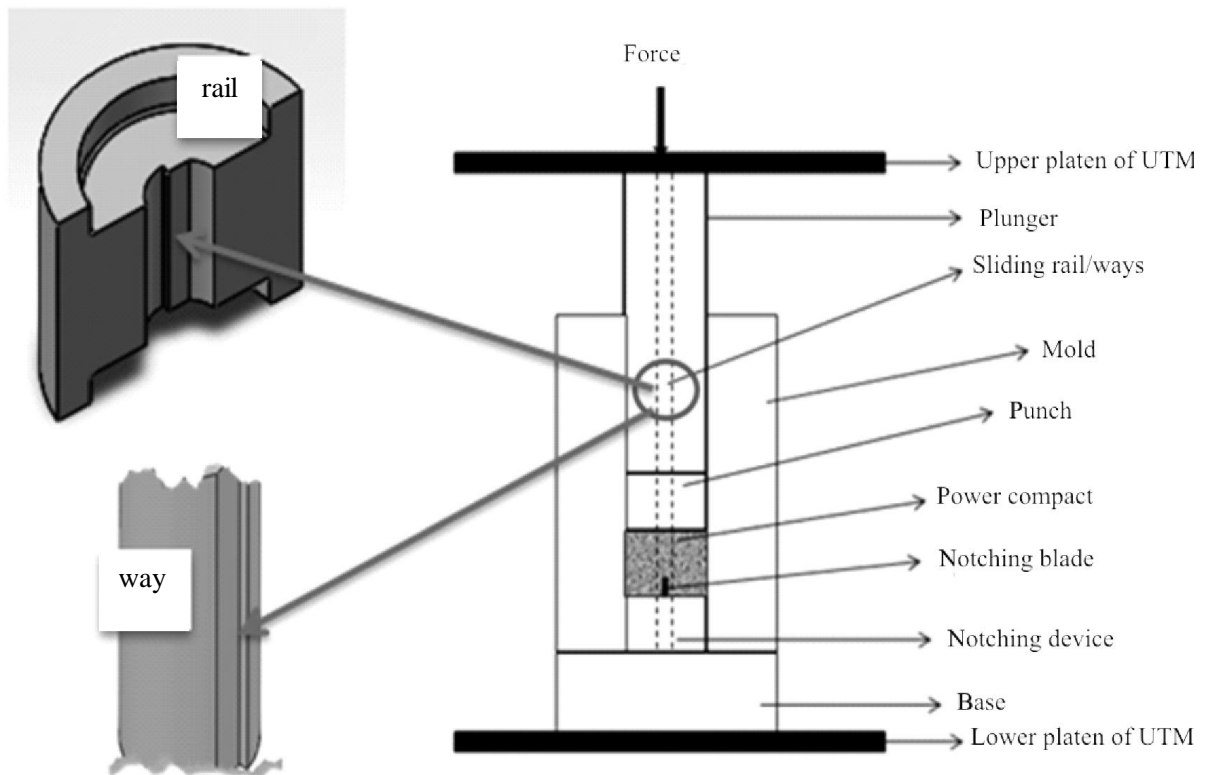


Figure 5: Schematic diagram of compaction die used for producing MDCTT compacts

The production of the MDCTT sample adopts an integrated uniaxial compression and notching technique. This method eliminates the need for machining of the test samples since the required notch on each sample is produced during the compaction process. A fixed mass of metal powder is compressed uniaxially in the die (see Figure 5) to produce the MDCTT sample shown in Figure 1. The die is equipped with a ‘rail’ and ‘ways’ that gives the MDCTT sample its unique feature.

In this study 15 g of metal powder was compressed uniaxially in the die at a rate of 2 mm/min until a fixed maximum pressure was attained. The maximum compaction pressures that were used are 206.87, 238.7, 270.53 and 302.36 MPa respectively. The procedure for producing each MDCTT sample is a standard sequence that begins with; fixing the mold onto the base of the die and lubricating the mold cavity. The lubricant used was magnesium stearate. Then carefully putting the notching device into the mold cavity (with the rail and way aligned) and transferring the 15 g of the metal powder into the cavity. The notching device was designed to cut a notch 1.2mm deep and 0.5 mm wide on each sample. The punch and the plunger are then lowered into the cavity with the punch making contact with the powder. Finally, the assembly of die and powder was then mounted on a 100 kN Instron 3383 universal testing machine (UTM) and compressed until one of the set maximum compaction pressure is reached (see Figure 5). The compressed powder or the powder compact of uniform diameter ($D = 20$ mm) is then ejected from the die. The thickness, t_2 and the mass, m_c of each compact were measured and recorded. All compacts that loss more than 0.02 g after ejection were rejected. The values reported are averages from five samples under the same compaction conditions.

The relative density, ρ_r of each sample of powder compact was computed from Equation (5) and Equation (6).

$$\rho_r = \frac{\text{Density of powder compact}}{\text{Density of Equivalent solid metal}} \quad (5)$$

$$\rho_r = \frac{m_c}{A_c t_2 \times \rho} \quad (6)$$

where, A_c is cross-section area of compact and ρ is the density of the equivalent solid metal.

Each of the MDCTT samples was compressed to fracture on the Instron UTM as shown in Figure 6.



Figure 6: MDCTT sample undergoing compression to fracture test

The profile of the fractured surfaces of the iron and copper powder compacts were captured under the lens of an LEO 1455 VP scanning electron microscope. The images were captured in the as-fractured state, no surface preparation or treatment was involved.

RESULTS AND DISCUSSION

Results

Table 2 presents the thickness of the MDCTT samples of the iron and copper powder after they were compressed to the pre-set maximum compaction pressures of 206.87, 238.70, 270.53 and 302.36 MPa respectively. The table also shows the values of the relative densities and the mode II fracture toughness for the iron powder compacts (IPC) and the copper powder compacts (CPC). These values were computed from Equation (4) and Equation (2) respectively. The density of iron metal was taken as 7.78×10^{-3} g/mm³ while that of copper metal was 8.96×10^{-3} g/mm³.

Figure 7 illustrates the trend between the compaction pressures and $\ln[1/(1-\rho_r)]$ for iron and copper powder compacts.

Figure 8 shows the influence of σ_c on the mode II fracture toughness of the iron powder compacts (IPC) and the copper powder compacts (CPC).

Figure 9 depicts the relationship between $\frac{1}{K_{IIc}}$ against $\frac{1}{1-\ln(\rho_r)^2}$ for the iron powder and the copper powder compacts while,

Figure 10 explains the behaviour of the lines of the graphs in Figure 9 at the point of intersection on the $\frac{1}{1-\ln(\rho_r)^2}$ axis.

Figure 11 to Figure 14 show the SEM morphology of the fractured surfaces of the IPC and CPC.

Table 2: Results of density and mode II fracture toughness for MDCTT compacts produced from iron and copper powders

Compaction Pressure, σ_c (MPa)	Iron Powder Compacts (IPC)			Copper Powder Compacts (CPC)		
	t_2 (mm)	ρ_r	K_{IIC} (MPa.m ^{0.5})	t_2 (mm)	ρ_r	K_{IIC} (MPa.m ^{0.5})
206.87	8.87	0.722	0.30	7.22	0.778	0.28
238.70	8.65	0.741	0.37	7.02	0.800	0.38
270.53	8.47	0.758	0.45	6.84	0.822	0.49
302.36	8.30	0.773	0.57	6.71	0.838	0.59

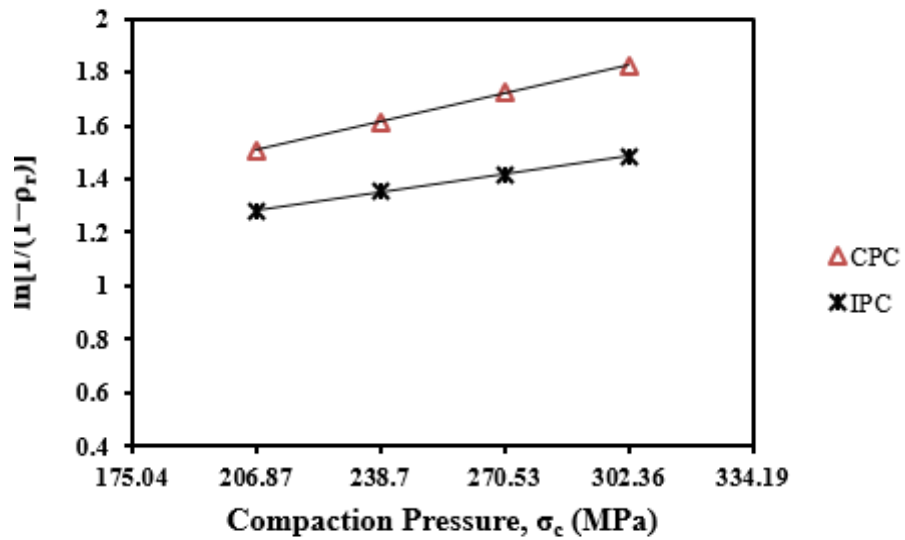


Figure 7: The effect of compaction pressure on $\ln [1/(1-\rho_r)]$ for MDCTT compacts of iron and copper powders

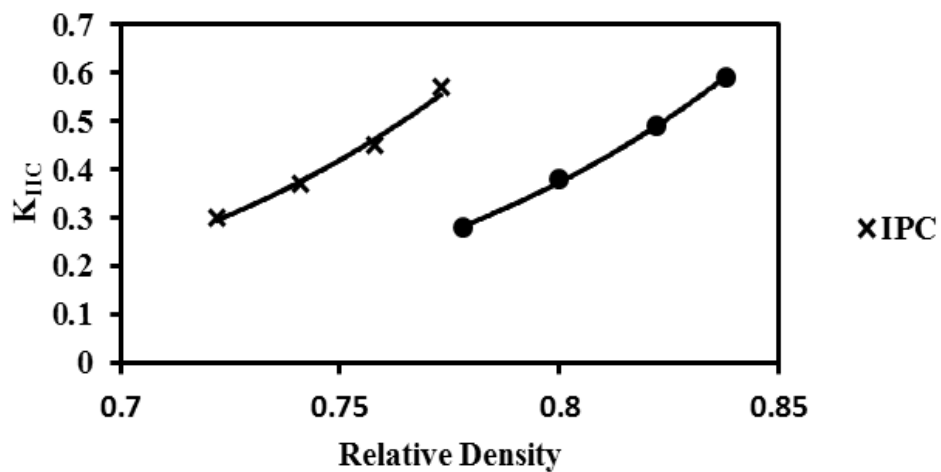


Figure 8: Effect of relative density on the mode ii fracture toughness of iron and copper powder compacts

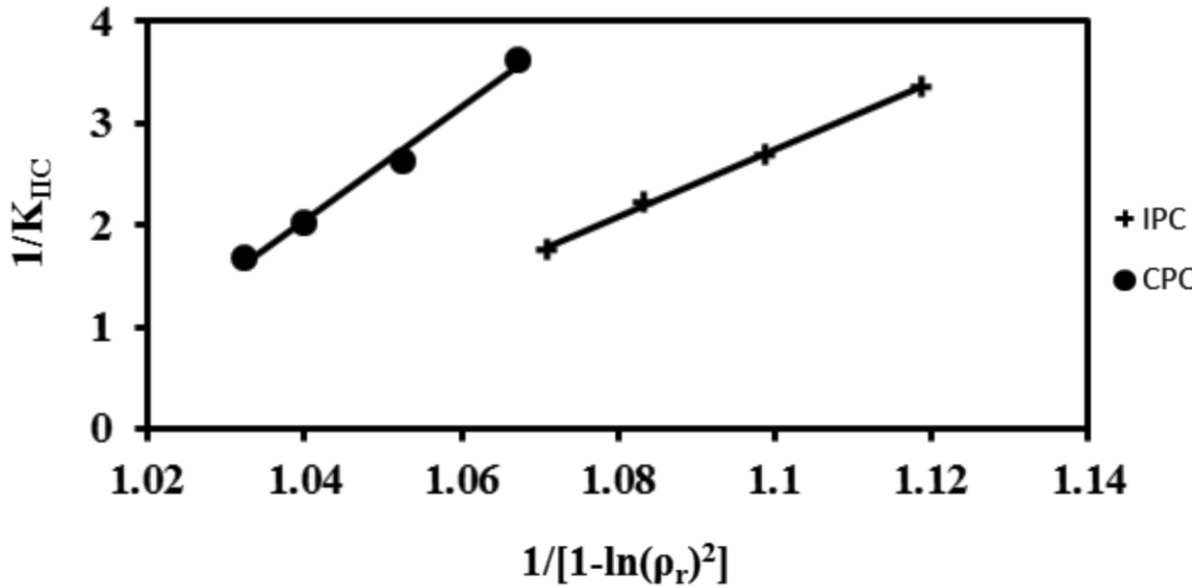


Figure 9: The graph of $\frac{1}{K_{IIIC}}$ against $\frac{1}{1-\ln(\rho_r)^2}$ for MDCTT compacts of iron and copper powders

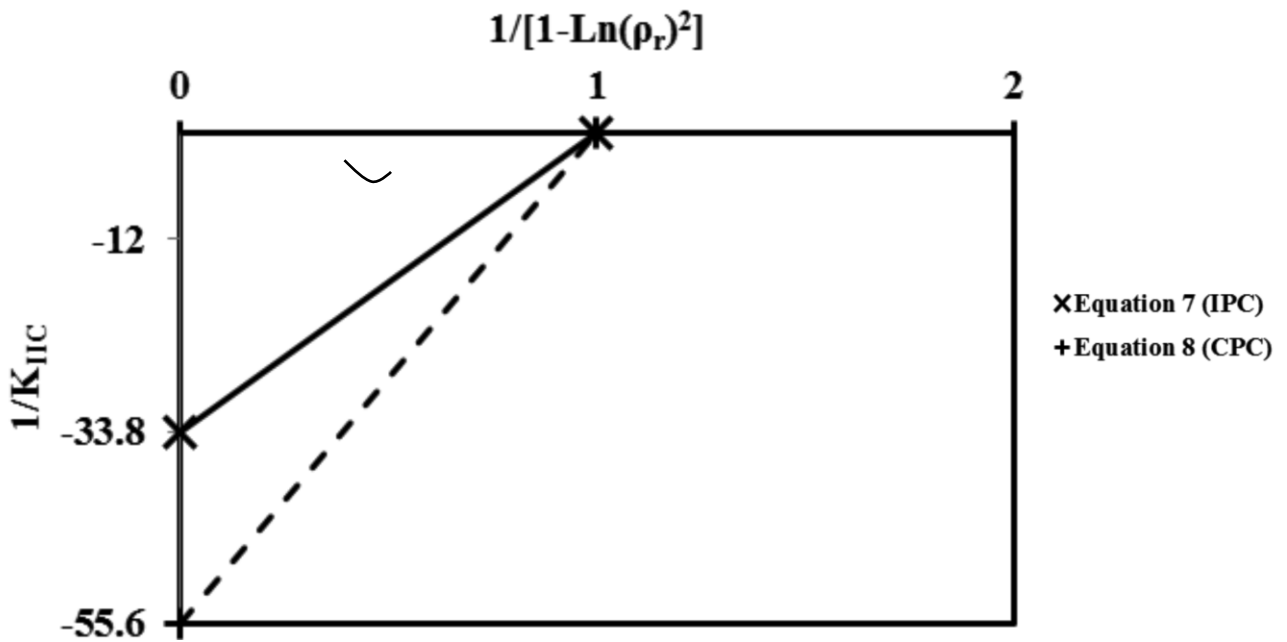


Figure 10: The Intersection between the Line of Equation 7 and the Line of Equation 8

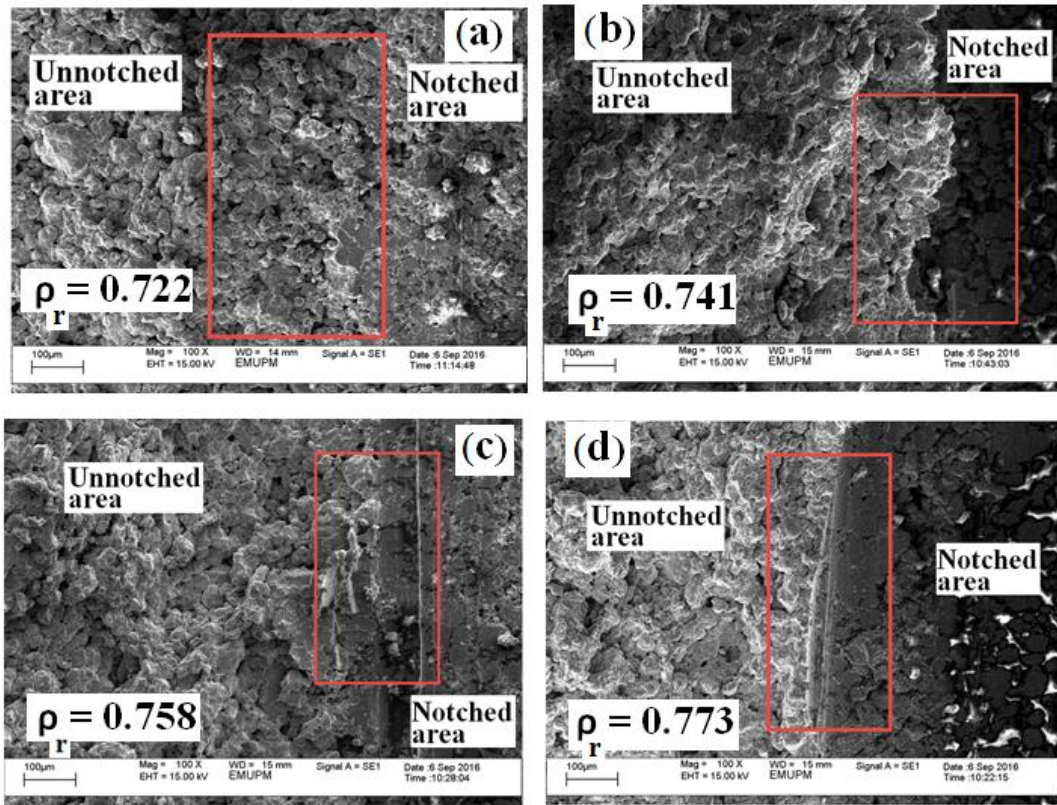


Figure 11: Effect of Relative Density on the Morphology at the Interface between the Notched and Unnotched Areas of Iron Powder Compact

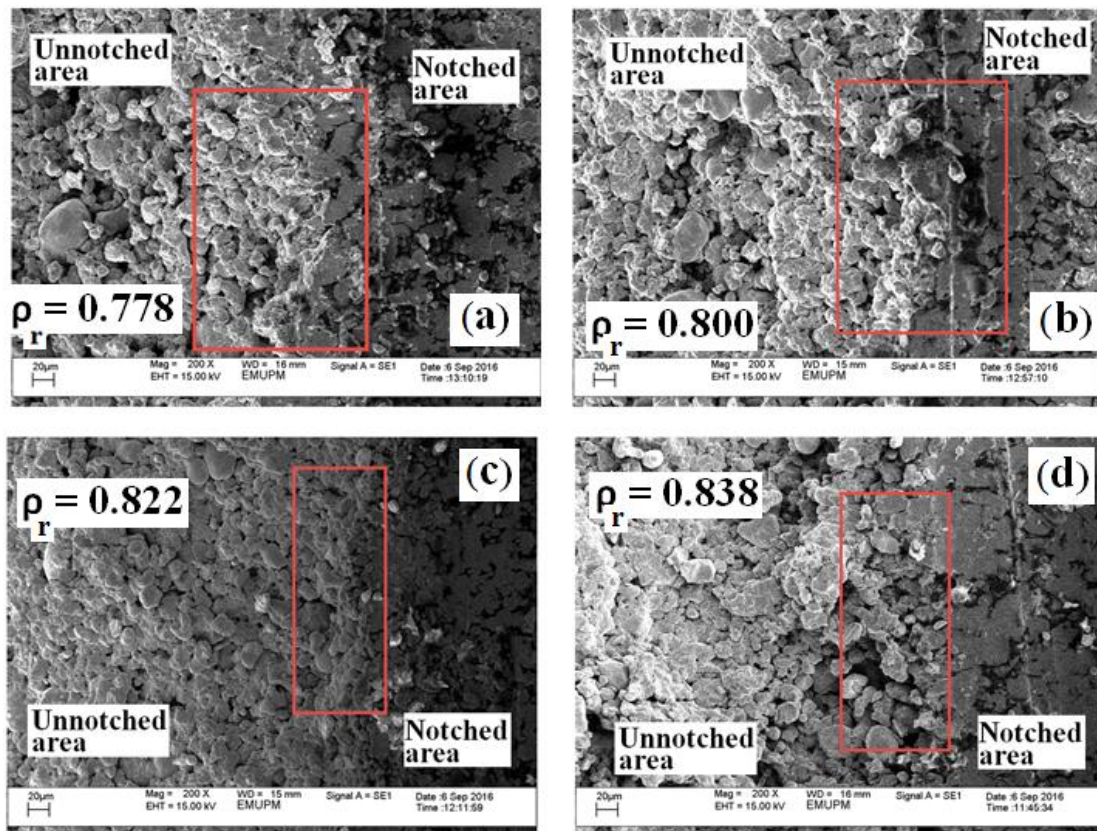


Figure 12: Effect of relative density on the morphology at the interface between the notched and unnotched areas of copper powder compact

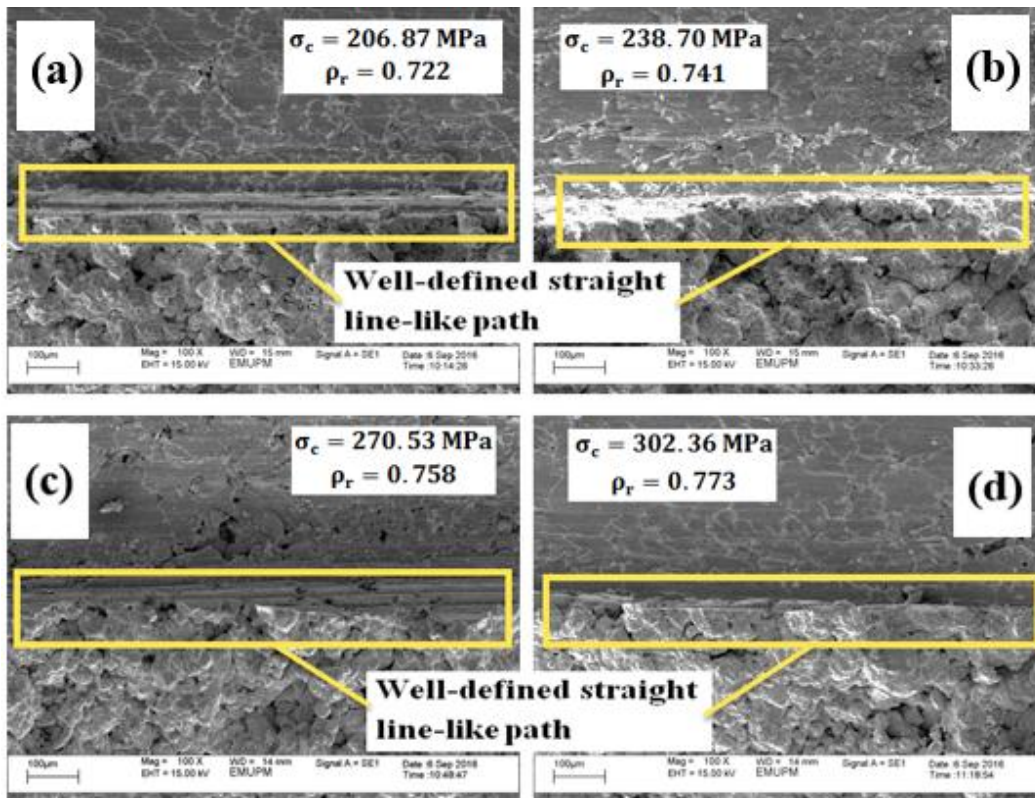


Figure 13: Fractured surfaces of MDCTT iron powder compacts of different relative density showing evidence of well-defined straight-line like (shear) failure

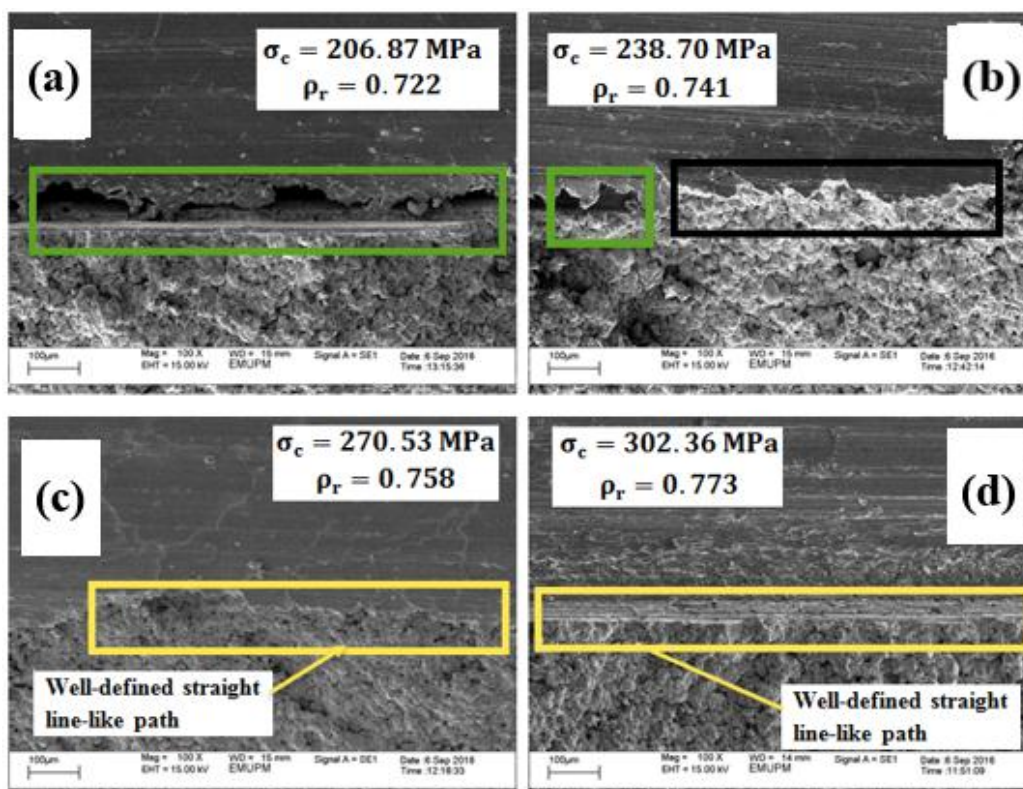


Figure 14: Fractured surfaces of MDCTT copper powder compacts of different relative density showing evidence of shear failure

DISCUSSION

It can be seen in Table 2 that the relative density of both powder compacts improve appreciably as the pressure rose from 206.87 MPa to 302.36 MPa. This trend agrees with the finding of Jonsén *et al.* (2007), Moon and Kim (1984), Hwang and Kobayashi (1990) and Heckel (1961).

Equation 7 and Equation 8 are straight line equations which define the relation between $\ln[1/(1-\rho_r)]$ and σ_c for the IPC and CPC respectively (Figure 7).

$$\ln \left[\frac{1}{(1-\rho_r)} \right] = 0.0033\sigma_c + 0.7558 \quad (7)$$

$$\ln \left[\frac{1}{(1-\rho_r)} \right] = 0.0021\sigma_c + 0.8225 \quad (8)$$

From Equation (7) the IPC line in Figure 7 was estimated to intersect the $\ln[1/(1-\rho_r)]$ axis at 0.76 while Equation (8) showed that the CPC line the same axis at 0.82. These values are close to 0.79 and 0.71 reported by Heckel (1961) for the same powders. According to Heckel findings, it is safe to compare the relative density of the MDCTT compacts to some of its other properties and draw meaningful inferences. Figure 8 compared the influence of the relative densities of the iron powder and the copper powder compacts on their respective mode II fracture toughness, K_{IIC} . The results depict that increased relative densities for each of the metal powder compacts led to improved K_{IIC} . The fracture toughness of the iron powder compacts was improved by 23.3%, 50% and 90% as the relative density of the compacts increased by 0.019, 0.036 and 0.051 respectively. While an improvement of 35.7%, 75% and 110% was recorded for copper powder compacts (CPC) for relative density rise of 0.022, 0.044 and 0.060 respectively. It can be inferred that the strength of the compacts has been boosted since one of the factors that enhance the strength of a PM component is improved green density (Jonsén *et al.*, (2007); Tahir and Ariffin (2006); Degnan *et al.* (2004); Lenel (1980). The green strength is due mainly to plastic deformation of powder particles (Hewitt *et al.*, (1974)) and mechanical fusion of the irregular surfaces of adjacent particles Anand and Mohan (2012); Lenel (1980). The trend in Figure 8 agreed with that reported by Tahir *et al.* (2010) and Tahir and Ariffin (2006) for iron powder compacts although they reported higher values relative density.

Figure 9 present an interesting behaviour observed in the metal powder compacts studied. Equation (9) and Equation (10) are unique equations derived when the reciprocal of K_{IIC} was plotted against $\frac{1}{1-\ln(\rho_r)^2}$ for the iron powder compacts and the copper powder compacts respectively.

$$\frac{1}{K_{IIC}} = 33.2 \frac{1}{1-\ln(\rho_r)^2} - 33.8 \quad (9)$$

$$\frac{1}{K_{IIC}} = 55.5 \frac{1}{1-\ln(\rho_r)^2} - 55.6 \quad (10)$$

It can be assumed from Equation (9) that the values of the slope and the intercept on the $\frac{1}{K_{IIC}}$ axis are equal, say 33.2 for the IPC. The same inference can be drawn for the CPC but its value is 55.5 (see Equation 10). Consequently, a generalized form of Equation (9) and Equation (10) can be written as Equation (11).

$$\frac{1}{K_{IIC\text{powder}}} = Q_{\text{powder}} \frac{1}{1-\ln(\rho_{r\text{powder}})^2} - Q_{\text{powder}} \quad (11)$$

where, $K_{IIC\text{powder}}$ and $\rho_{r(\text{powder})}$ are the fracture toughness and relative density of a given metal powder compact and Q_{powder} is a constant which describes a property of a metal powder compact. This property could be related to one or more of the properties of metal powders or metal powder compacts. Furthermore, Figure 10 depicts the points of intersection of the lines on Figure 9 with the $\frac{1}{K_{IIC}}$ and the $\frac{1}{1-\ln(\rho_r)^2}$ axes.

Theoretically, the lines of the IPC and CPC intersect each other on the $\frac{1}{1-\ln(\rho_r)^2}$ axis. This point of intersection is defined by Equation (12).

$$\left(\frac{1}{1-\ln(\rho_r)^2}, \frac{1}{K_{IIC}} \right) = (1, 0) \quad (12)$$

From the first part of Equation 12, we obtained Equation (13) and Equation (14)

$$1 - \ln(\rho_r)^2 = 1 \quad (13)$$

$$\text{Hence, } \rho_r = 1 \quad (14)$$

To satisfy the second part of Equation (12), Equation (15) must be true

$$K_{IIC} \gg 1 \quad (15)$$

Equation (14) and Equation (15) gave the two conditions that have to be fulfilled before the two lines in Figure 10 could meet.

Equation (14) implies that at the point of intersection on Figure 10, the density of the iron powder compact was the same as that of iron metal and the density of the copper powder compacts was equal to the density of copper metal. Experimentally, it is difficult to press metal powders to achieve the same density as their parent solid metals. At a compaction pressure of 600 MPa, the green density of iron powder was 7.13 g/cm³ Alabi *et al.* (2016). This value is lower than the density of solid iron metal which is 7.87 g/cm³ Cambridge University (2003). The highest density of copper powder compact that was reported in literature is 8.3 g/cm³ Ngai *et al.* (2005). This value is also less than the 8.96 g/cm³ for solid copper metal. Consequently, at the point of intersection on the $\frac{1}{1-\ln(\rho_r)^2}$ axis on Figure 10, the iron and copper metal powder compacts must have metamorphosed to solid metals. This explains Equation (15). Higher values of K_{IIC} are consistent with the values of solid iron and copper as deduced from the values of the K_{IC} reported in Cambridge University materials data book (2003). The K_{IC} of cast iron

was reported to range from 22 and 54 MPa.m^{0.5} while that of copper alloy ranged from 30 to 90 MPa.m^{0.5}. Applying the SED- criterion ratio of $\frac{K_{IIC}}{K_{IC}} = 1.04$, Sih (1974), the values of K_{IIC} for the cast iron and the copper alloy are definitely much greater than 1.0 MPa.m^{0.5}. The highest value of K_{IIC} obtained for both iron and copper powder compacts was less than 1.0 MPa.m^{0.5} as shown in Table 2.

Another point of interest in Figure 10 is the angle θ which the two lines make at the point of intersection. The value of this angle is calculated as shown in Equation (16).

$$\theta = \tan^{-1}(55.6) - \tan^{-1}(33.8) \quad (16)$$

Hence, $\theta = 0.70$

It was noticed that the value of θ is the same as the ratio of the coefficient of thermal expansivity for pure iron metal and pure copper metal, 11.70: 16.50 Technologies (2007); Oberg (2012).

If Equation (16) is related to Equation (11), a generalized form of Equation (16) can be written as Equation (17).

$$\theta = \tan^{-1} Q_{\text{copper powder}} - \tan^{-1} Q_{\text{iron powder}} \quad (17)$$

Hitherto, mathematical equations and graphs from experimental data have been used to show that enhancing the relative density of metal powder compact leads to higher fracture toughness. In the next paragraph, the structures of the fracture surfaces of the metal compacts are used to show how improved compact density slows down the rate of crack extension.

Figure 11 and Figure 12 show the morphology of the fractured surfaces of MDCTT compacts produced from iron and copper powder respectively. The integrated compaction-notching method made it possible to see a distinct separation between the notched and unnotched areas. A portion of the separation is shown on each of the micrographs by the red rectangle. The area is in the vicinity of the tip of the notch, the region where crack extension begins. The images in Figure 11 and Figure 13 have magnifications of 100 while those in Figure 12 and Figure 14 have magnification of 200. The copper powder had finer particle sizes than the iron powder (see Table 1). This might be responsible for the inability to capture clear images of the CPCs at the magnification of 100. All the images were captured using a scanning electron microscope.

The fractured surface pattern for the compacts of iron powder (Figure 13) and the copper powder (see Figure 14) shows straight line-like paths which are more defined in the samples with higher densities. The straightness of the fractured path seen in the IPCs shown in Figure 13 is an indication that the failure was due to shear. For the CPCs, Figure 14 (c) and (d) show samples with better formed straight line-like fractured surfaces. The area covered by the yellow rectangles in Figure 14 (d) indicated the clearest evidence of shear failure, and it is for the sample with the highest relative density, 0.773. It is likely that the poor definition of straightness in the portion of the failed surfaces

shown in the green rectangles (Figure 14 (a) and (b)) were affected by relatively lower density. Therefore, it can be concluded that the cause of the fractured failure in the MDCTT samples produced from the iron and the copper powders is shear force.

CONCLUSIONS

The relationship between the mode II fracture toughness, K_{IIC} and the relative density of iron powder compacts and copper powder compacts have been successfully studied using experimental method. The MDCTT samples used were produced from the integrated uniaxial compaction of loose powders. The values of the K_{IIC} for the iron and copper powder compacts were found to increase as the powders become denser. This implies that the rate of crack propagation in the compacts decreases with improved densification. The developed mathematical equation, $\frac{1}{K_{IIC\text{powder}}} = Q_{\text{powder}} \frac{1}{1 - \ln(\rho_{\text{rpowder}})^2} - Q_{\text{powder}}$, which relates the mode II fracture toughness for the metal powder studied to the relative density also has the potential of defining more useful properties of the iron and copper powder compacts.

ACKNOWLEDGEMENT

This study was supported by grants from the Universiti Putra Malaysia (GP-IPS/2015/9452300) and the Ministry of Higher Education Malaysia (03-01-15-1758FR)

REFERENCES

- Akseli, I., Iyer, S., Lee, H. P., Cuitiño and A. M., 2011. A Quantitative Correlation of the Effect of Density Distributions in Roller-Compacted Ribbons on the Mechanical Properties of Tablets Using Ultrasonics and X-ray Tomography. *AAPS PharmSciTech* 12, 834–853. doi:10.1208/s12249-011-9640-z.
- Alabi, A. A., Tahir, S. M., Zahari, N. I., Azmah Hanim, M. A., Anuar and M. S., 2017. A modified diametrical compression test technique (MDCTT) for mode II fracture toughness of iron powder compact. *Powder Technol.* 319, 356–364. doi:10.1016/j.powtec.2017.06.058.
- Alabi, A. A., Tahir, S. M., Zahari, N. I., Azmah Hanim, M. A. and Anuar, M. S., 2016. Effect of Notching Face on Fracture Toughness of Green Metal Powder Compacts. *Glob. J. Eng. Technol. Rev.* 1, 49–56.
- Anand, S. S. and Mohan, B., 2012. Effect of Particle Size, Compaction Pressure on Density and Mechanical Properties of Elemental 6061Al Alloy through Powder Metallurgical Process. *Int. J. Mater. Eng. Innov.* 3, 259–268. doi:10.1504/IJMATEL.2012.049265.
- ASTM E1820-01, 2001. Standard Test for Measurement of Fracture Toughness. *ASTM Int.* 1–46. doi:10.1520/E1820-09.2.
- Cambridge University, 2003. *Materials Data Book*, 2003 Editi. ed. Cambridge University Engineering Department.

- Chen, M., Yin, Z., Yuan, J., Xu, W., Ye, J. and Yan, S., 2018. Microstructure and Properties of a Graphene Platelets Toughened Boron Carbide Composite Ceramic by Spark Plasma Sintering. *Ceram. Int.* 0–1. doi:10.1016/j.ceramint.2018.05.188.
- Clobes, J. K., Green and D. J., 2002. Validation of Single-Edge V-Notch Diametral Compression Fracture Toughness Test for Porous Alumina. *J. Mater. Sci.* 37, 2427–2434. doi:10.1023/A:1015414917833.
- Degnan, C. C., Kennedy, A.R., Shipway, P.H., 2004a. Fracture Toughness Measurements of Powder Metallurgical (P/M) Green Compacts: A Novel Method of Sample Preparation. *J. Mater. Sci.* 39, 2605–2607. doi:10.1023/B:JMSC.0000020039.84002.
- Degnan, C. C., Shipway, P. H., Kennedy, A. R., 2004b. Comparison of the Green Strength of Warm Compacted Astaloy CrM and Distaloy AE Densmix* Powder Compacts. *Mater. Sci. Technol.* 20, 731–738. doi:10.1179/026708304225017292.
- Enneti, R. K., Lusin, A., Kumar, S., German, R. M., Atre, S. V., 2013. Effects of Lubricant on Green Strength, Compressibility and Ejection of Parts in Die Compaction Process. *Powder Technol.* 233, 22–29. doi:10.1016/j.powtec.2012.08.033.
- Farahbakhsh, I., Ahmadi, Z., Shahedi Asl, M., 2017. Densification, Microstructure and Mechanical Properties of Hot Pressed ZrB₂-SiC Ceramic Doped with Nano-Sized Carbon Black. *Ceram. Int.* 43, 8411–8417. doi:10.1016/j.ceramint.2017.03.188.
- Fleck, N. A., Smith, R. A., 1981. Effect of Density on Tensile Strength, Fracture Toughness, and Fatigue Crack Propagation Behaviour of Sintered Steel. *Powder Metall.* 24, 121–125. doi:10.1179/pom.1981.24.3.121.
- Garner, S., Ruiz, E., Strong, J., Zavaliangos, A., 2014. Mechanisms of Crack Formation in Die Compacted Powders during Unloading and Ejection: An experimental and Modeling Comparison between Standard Straight and Tapered Dies. *Powder Technol.* 264, 114–127. doi:10.1016/j.powtec.2014.04.086.
- Guha Roy, D., Singh, T. N., Kodikara, J., Talukdar, M., 2017. Correlating the Mechanical and Physical Properties with Mode-I Fracture Toughness of Rocks. *Rock Mech. Rock Eng.* 50, 1941–1946. doi:10.1007/s00603-017-1196-0.
- Hare, C., Bonakdar, T., Ghadiri, M., Strong, J., 2018. Impact Breakage of Pharmaceutical Tablets. *Int. J. Pharm.* 536, 370–376. doi:10.1016/j.ijpharm.2017.11.066.
- He, J., Shao, Z., Khan, D. F., Yin, H., Elder, S., Zheng, Q., Qu, X., 2018. Investigation of Inhomogeneity in Powder Injection Molding of Nano Zirconia. *Powder Technol.* 328, 207–214. doi:10.1016/j.powtec.2017.12.075.
- Heckel, R. W., 1961. Density-Pressure Relations in Powder Compaction. *Trans. Metall. Soc. AIME* 221, 671–675.
- Hewitt, R. L., Wallace, W., DeMalherbe, M.C., 1974. Plastic Deformation in Metal Powder Compaction. *Powder Metall.* 17. doi:10.1007/978-3-319-48163-0_12.
- Hwang, B. B., Kobayashi, S., 1990. Deformation Characterization of Powdered Metals in Compaction. *Int. J. Mach. Tools Manuf.* 30, 309–323. doi:10.1016/0890-6955(90)90139-A.
- Jonsén, P., Häggblad, H. Å., Troive, L., Furuberg, J., Allroth, S., Skoglund, P., 2007. Green Body Behaviour of High Velocity Pressed Metal Powder. *Mater. Sci. Forum* 534–536, 289–292. doi:10.4028/www.scientific.net/MSF.534-536.289.
- Khuntia, S. K., Pani, B. B., 2018. Powder Metallurgy Processing of Low Carbon Content Ferrous Powders for Making Structural Components. *Int. J. Mater. Sci.* 13, 7–14.
- King, P., Poszmik, G., Causton, R., 2005. Higher Green Strength Materials for Green Handling, in: *PM2Tec2005*. Montreal, Canada.
- Lenel, F. V, 1980. *Powder Metallurgy: Principles and Applications*. Metal Powder Industries Federation, New Jersey.
- May, R. K., Su, K., Han, L., Zhong, S., Elliott, J.A., Gladden, L.F., Evans, M., Shen, Y., Zeitler, J.A., 2013. Hardness and Density Distributions of Pharmaceutical Tablets Measured by Terahertz Pulsed Imaging. *J. Pharm. Sci.* 102, 2179–2188. doi:10.1002/jps.23560.
- Moon, I., Kim, K., 1984. Relationship between Compacting Pressure, Green Density, and Green Strength of Copper Powder Compacts. *Powder Metall.* 27, 80–84. doi:10.1179/pom.1984.27.2.80.
- Moshtaghioun, B. M., Cumbreira-Hernández, F. L., Gómez-García, D., de Bernardi-Martín, S., Domínguez-Rodríguez, A., Monshi, A., Abbasi, M.H., 2013. Effect of Spark Plasma Sintering Parameters on Microstructure and Room-Temperature Hardness and Toughness of Fine-Grained Boron Carbide (B₄C). *J. Eur. Ceram. Soc.* 33, 361–369. doi:10.1016/j.jeurceramsoc.2012.08.028.
- Moshtaghioun, B. M., Gomez-Garcia, D., Dominguez-Rodriguez, A., Todd, R.I., 2016. Grain Size Dependence of Hardness and Fracture Toughness in Pure Near Fully-Dense Boron Carbide Ceramics. *J. Eur. Ceram. Soc.* 36, 1829–1834. doi:10.1016/j.jeurceramsoc.2016.01.017.
- Ngai, T. L., Wang, S., Li, Y., Zhou, Z., Chen, W., 2005. Warm Compaction of Powder Metallurgy of Copper. *Trans. Nonferrous Met. Soc. China* 15, 77–81.
- Oberg, E., 2012. *Machinery's Handbook*. Industrial Press Inc, Connecticut.

- Poquillon, D., Lemaitre, J., Tailhades, P., Lacaze, J., 2002. Cold Compaction of Iron Powders — Relations between Powder Morphology and Mechanical Properties Part I: Powder Preparation and Compaction. *Powder Technol.* 126, 65–74.
- Quinn, G. D., Bradt, R. C., 2007. On the Vickers Indentation Fracture Toughness Test. *J. Am. Ceram. Soc.* 90, 673–680. doi:10.1111/j.1551-2916.2006.01482.x.
- Rocha-Rangel, E., 2011. Fracture Toughness Determinations by Means of Indentation Fracture, in: Cuppoletti, J. (Ed.), *Nanocomposites with Unique Properties and Applications in Medicine and Industry*. In Tech, Croatia, pp. 21–38. doi:10.5772/18127.
- Sairam, K., Sonber, J. K., Murthy, T.S.R.C., Subramanian, C., Fotedar, R.K., Nanekar, P., Hubli, R.C., 2014. Influence of Spark Plasma Sintering Parameters on Densification and Mechanical Properties of Boron Carbide. *Int. J. Refract. Met. Hard Mater.* 42, 185–192. doi:10.1016/j.ijrmhm.2013.09.004.
- Shi, J., Cheng, Z., Gelin, J. C., Barriere, T., Liu, B., 2017. Sintering of 17-4PH stainless Steel Powder Assisted by Microwave and the Gradient of Mechanical Properties in the Sintered Body. *Int. J. Adv. Manuf. Technol.* 91, 2895–2906. doi:10.1007/s00170-016-9960-y.
- Sih, G. C., 1974. Strain-Energy-Density Factor Applied to Mixed Mode Crack Problems. *Int. J. Fract.* 10, 305–321.
- Solimanjad, R., Larsson, N., 2003. Die Wall Friction and Influence of Some Process Parameters on Friction in Iron Powder Compaction. *Mater. Sci. Technol.* 19, 1777–1782.
- Szendi-Horvath, G., 1980. Fracture Toughness Determination of Brittle Materials Using Small to Extremely Small Specimens. *Eng. Fract. Mech.* 13, 955–961.
- Tahir, S. M., Ariffin, A. K., 2006a. Simulation of Crack Propagation in Metal Powder Compaction. *Int. J. Comput. Methods Eng. Sci. Mech.* 7, 293–302. doi:10.1080/15502280600549363.
- Tahir, S. M., Ariffin, A. K., 2006b. Fracture in Metal Powder Compaction. *Int. J. Solids Struct.* 43, 1528–1542. doi:10.1016/j.ijsolstr.2005.10.010.
- Tahir, S. M., Ariffin, A. K., Anuar, M. S., 2010. Finite Element Modelling of Crack Propagation in Metal Powder Compaction Using Mohr-Coulomb and Elliptical Cap Yield Criteria. *Powder Technol.* 202, 162–170. doi:10.1016/j.powtec.2010.04.033.
- Technologies, A., 2007. Material Expansion Coefficients, in: *Agilent Laser and Optics User's Manual, Volume I*. California, pp. 280–290.
- Xiaorong, Z., Gao, H., Zhang, Z., Wen, R., Wang, G., Mu, J., Che, H., Zhang, X., 2017. Effects of Pressure on Densification Behaviour, Microstructures and Mechanical Properties of Boron Carbide Ceramics Fabricated by Hot Pressing. *Ceram. Int.* 43, 6345–6352. doi:10.1016/j.ceramint.2017.02.043.
- Yohannes, B., Gonzalez, M., Abebe, A., Sprockel, O., Nikfar, F., Kang, S., Cuitino, A.M., 2015. The Role of Fine Particles on Compaction and Tensile Strength of Pharmaceutical Powders. *Powder Technol.* 274, 372–378. doi:10.1016/j.powtec.2015.01.035.
- Zhou, M., Huang, S., Hu, J., Lei, Y., Xiao, Y., Li, B., Yan, S., Zou, F., 2017. A Density-Dependent Modified Drucker-Prager Cap Model for Die Compaction of Ag_{57.6}-Cu_{22.4}-Sn₁₀-In₁₀ Mixed Metal Powders. *Powder Technol.* 305, 183–196. doi:10.1016/j.powtec.2016.09.061